Fita Fernández, IC.; Cruz González, JM.; Calvo Muñoz, C.; Soriano Martinez, L.; Paya Bernabeu, JJ.; Sánchez Martín, I. (2018). Drying-rewetting cycles in ordinary Portland cement mortars investigated by electrical impedance spectroscopy. Construction and Building Materials. 187:954-963. doi:10.1016/j.conbuildmat.2018.07.227

Drying-rewetting cycles in ordinary Portland cement mortars investigated by electrical impedance spectroscopy

I.C. Fita[1*]; J.M. Cruz[1]; C. Calvo[2]; L. Soriano[2]; J. Payá[2]; I. Sánchez[3]

[1] Departamento de Física Aplicada, Universitat Politècnica de València, Camino de Vera s/n, 46022 Valencia, Spain.

[2] ICITECH, Instituto de Ciencia y Tecnología del Hormigón, Universitat Politècnica de València, Camino de Vera s/n, 46022 Valencia, Spain.

[3] Departamento de Ingeniería Civil. Universidad de Alicante, Carretera San Vicente del Raspeig s/n, 03690 San Vicente del Raspeig, Spain

* corresponding author: Tel. 34 96 387 95 22, e-mail address: infifer@fis.upv.es

ABSTRACT

Changes caused in the porous microstructure of ordinary Portland cement (OPC) mortars were studied using electrical impedance spectroscopy (EIS) and equivalent circuit (EqC). Two successive processes, at 20 ºC and 50 °C, consisting of several drying-rewetting cycles, were applied to the mortars. After each cycle, the electrical impedance and the amount of water absorbed were measured. The EIS-EqC methodology allowed to find two distributed impedance relaxations, associated to capillary and gel-C-S-H porosities, respectively. At room temperature any microstructural change was not detected. Nevertheless, at 50 °C two microstructural changes were inferred: 1) the volume of accessible porosity increased (pore coarsening) and 2) the surface of the conductive path through C-S-H gel became more conductive (surface smoothing).

Key words: mortar, gel-porosity, capillary-porosity, drying-rewetting, electrical-impedance-spectroscopy.

1. INTRODUCTION

The physical properties of the pore network in hardened cement-based materials (HCB), such as pastes, mortars and concretes, determine their fundamental engineering properties, such as mechanical strength and durability. The pore network can be characterized by a complex function of its pore size, pore shape, pore surface area, volume fraction of pores, connectivity between pores and water saturation level. In mature HCB materials, the pores that contain non-bound liquid water are classified into three classes of porosity, with decreasing size and with different pore shape: i) capillary porosity (> 8 nm in diameter) that includes inter-hydrate spaces 8-20 nm, ii) gel porosity (large pores ≈ 8-4 nm in diameter and small pores ≈ 4-2 nm in diameter) and iii) interlayer porosity (< 2nm in width). Henceforth, gel porosity (GeP) will be the volume of pores associated with the C-S-H gel, whose size is less than 8 nm, and capillary porosity (CaP) will refer to the pores greater than 8 nm.

The transition between percolation and depercolation of CaP (communicated or interrupted by the gel C-S-H, respectively) has implications on water curing, transport properties and the durability response of HCB structures. The relationship between the depercolated state and CaP volume has been studied in several ways [1]. The investigation of removing water from HCB materials through drying-rewetting processes is a method for assessing the durability, and is also a useful approach for characterizing different parameters of the pore structure [2].

The intensity of drying depends on the temperature, ambient relative humidity (RH%) and duration of the process. Each drying intensity affects the porosity down to a certain pore size, but the movement of water in these pores alters the redistribution of water in the pores of smaller sizes [3]. Some important features about water displacement and changes in the porosity of HCB materials, subjected to drying processes, are reported in the literature. The most remarkable results at different temperatures are:

1) Drying at 60 ^{o}C:
   a. the cement paste exhibited a coarsening of capillary porosity (increasing the mean size pore) and a collapse of low-density C-S-H gel [4-6].
   b. for 14 days, the mortar lost the water of capillary and gel porosity, but not that of the interlayer porosity [3].
   c. the mortar removed a large fraction of water from the interlayer porosity, but did not at 40 ^{o}C [7].
2) Oven-drying of HCB materials at 105 ^{o}C for 24 hours was used as a reference method for removing completely the non-bound water [8,9].
3) Drying at room temperature and relative humidity RH > 25% was shown to be a reversible process regards to the water content, because the water in the

interlayer pores did not move and the water in gel and capillary pores could return after saturation [10]. Drying at room temperature and RH = 0%, and subsequent re-saturating, made the gel particles closer [11].

Several methods have been used to measure changes in the porosity of HCB materials after drying treatments:

1) H-NMR (nuclear magnetic resonance) can evaluate quantitatively the percentages of remaining water [8]. It is also possible to calculate the ratio surface/volume of pores [12] and the gel pore size [3,7,13].
2) SANS (small-angle neutron scattering) gives a direct measurement of i) total internal surface area accessed by mobile water, ii) volume fractal and iii) surface fractal. The first fractal parameter is associated to the packing of C-S-H gel particles, and the second one can be associated with the roughness of the cement grains [2,11,14].
3) WVSI (water vapour sorption isotherms) allows to relate the mass water content to the RH% conditions and the minimum size of saturated pores [6,9,10,15].
4) MIP (mercury intrusion porosimetry) gives a pore size distribution after a drying process [16-18].
5) EIS (electrical impedance spectroscopy) has been used to evaluate the effect of drying on microstructural changes in HCB materials, but only in a few articles [19,20]. The pore coarsening due to drying treatment was related to the size of the frequency arc in the impedance plot. The presence of an intermediate arc in the impedance plot was associated with the formation of denser phases and new interfacial regions between collapsing C-S-H surfaces. However, quantitative analysis was not performed.

The main advantages of the EIS method are twofold: samples can be measured without previous treatments, and the measurement process is non-destructive and non-invasive. The usefulness of EIS (up to 1 MHz), when applied to saturated HCB materials, is that their response shows the ionic conductivity in the pores, distinguishing between the bulk space and the surface.

During the last 20 years, EIS in the range of 1 Hz to 1 MHz has been used in HCB materials in order to relate the electrical macroscopic properties to the microstructure [20-38]. In the following paragraphs a brief review related to the EIS technique and the equivalent electrical circuit (EqC) method, applied to impedance data performed in a two-electrode conductive cell, is presented.

The EqC method is based on the configuration of an electrical circuit with passive electrical elements such as resistance R, capacitor C, and constant phase element Q. These elements are connected in series, in parallel or in other arrangement, in order to fit experimental impedance data to theoretical impedance of the circuit, in the frequency range of the experiment.

The admittance of Q is frequency dependent: $Y(Q) = Y_0\,(j\cdot 2\pi\cdot f)^n$, characterized by two parameters Y_0 and n (where f is the frequency and j the complex imaginary unit). This complex admittance has two components:

$$ReY(Q) = Y_0\omega^n \cdot \cos(n\frac{\pi}{2}) \quad (1a)$$

$$ImY(Q) = Y_0\omega^n \cdot \mathrm{sen}(n\frac{\pi}{2}) \quad (1b)$$

Circuits with three branches in parallel have been proposed [39-42], being represented as $(R_1Q_1[R_2Q_2])$ following the circuit description code (CDC) [43]. This parallel circuit represents three main phases of the material with different types of conductivity (with respect to the applied voltage): resistive (R_1, in phase), capacitive (Q_1, out of phase $n_1\cdot\pi/2$ radians) and resistive-capacitive in series (R_2Q_2, lagged $< n_2\cdot\pi/2$ radians). This three-branch circuit has the advantage that allows to identify three different phases of the material and to monitor their evolution. However, its weakness is that other alternative circuits with different number of branches in parallel also allow to explain the bulk electrical conductivity.

Recently, a circuit with two Randles in series: R_s (C_1 [R_1W_1]) (C_2 [R_2W_2]) has been applied [21,37,44,45], being W a Warburg element equivalent to a Q element with n=1/2.

A general circuit for fitting the experimental data, without the need of a priori assumptions, is a Voigt circuit with a certain number of pairs elements in parallel (RC) connected in series. Any set of impedance data can be fitted to a circuit with sufficient number of (RC) [46-49]. This circuit also serves to: i) check if the experimental data fulfil the Kramers-Kronig relations, ii) obtain the time constant of each (RC) (τ = RC) and iii) estimate continuous distributions with some approximate results [46].

If the material system has continuous impedance relaxations, as it is the case of HCB materials, a series circuit with different pairs of (RQ) elements can be used. Each (RQ) represents a different distributed relaxation of the impedance [47-49]. The characteristic time constant T of the distributed relaxation is defined as [22]:

$$T = (R \cdot Y_0)^{(1/n)} \qquad (2)$$

Some researchers found a single relaxation (RQ) in OPC mortars [26,50], and also in cement pastes [51]. Other authors presented two relaxations, $(R_1Q_1)(R_2Q_2)$ in OPC mortars [52,53], and even a single relaxation in series with a resistance has been proposed, $R_1(R_2Q_2)$ [54].

A common feature in these investigations with saturated mortars is the presence of a distributed relaxation (RQ) with an exponent n of Q close to 0.80. This exponent n represents the width of the distributed relaxation in the frequency dimension. The value n = 1 corresponds to a narrow Debye relaxation and a decreasing value of n (from 1 to 0.5) means an increase in the width of the relaxation. The exponent n = 0.80 has been related to: i) the fractal dimension of the C-S-H gel [26,50,51], ii) the ratio of dielectric/conductive components in the admixture that constitutes the C-S-H gel [42,55] and iii) the water confined in nanometer size pores [56]. Whatever its meaning is, a change of n depicts a change in the structure of the gel C-S-H in HCB materials.

The main objective of this paper is to establish the methodology EIS-EqC to assess the changes in microstructure of OPC mortars subjected to several cycles of drying at low intensity conditions (20 ºC and 50 ºC) and subsequent resaturating.

Given the controversy about the number of relaxations in saturated mortars, and in order to facilitate comparability of future studies, one specific objective of this work aims to demonstrate that electrical conductivity of saturated OPC mortars can be characterised by two impedance relaxations of type (RQ). This physical model is validated with the applicability of the same EqC to all saturated states, the original and the resultant states after the successive drying-rewetting cycles throughout the experiment. The relation between the two relaxations and the main two porosities, CaP and GeP, is discussed by analysing the amount of water removed-absorbed in the drying-rewetting cycles.

2. EXPERIMENTAL

2.1 Materials

Mortar samples were prepared using ordinary Portland cement (OPC) of the type CEM I 52.5R according to the composition, specifications and conformity criteria standard UNE-EN 197-1:2011 [57].

To obtain mortars of different porosities, three different w/c ratios were used: 0.40, 0.50 and 0.60 labelled as m040, m050 and m060, respectively. The aggregate-to-cement ratio (a/c) was 3/1 (62% in volume). Siliceous sand with a fineness modulus of 4.1 was used as the aggregate.

Mortar specimens were prepared according to European standard UNE-EN 196-1:2005 [58]. Fresh mortar was cast into prismatic moulds measuring 4 x 4 x 16 cm^3. Specimens were cured at temperatures of t = 20 ± 2 ºC and a relative humidity RH > 99% for 24 hours. After demoulding, samples were immersed in a saturated lime solution and were cured in this environment at 20 ºC for 270 days. Three samples of each mortar were prepared for impedance measurements.

2.2 Methods

2.2.1 Impedance measurements

Mature mortars, 270 days old, were measured by EIS before and after each drying-rewetting cycle, always in saturated state.

The electrical impedance measurements were performed with the impedance meter HP-4284A (impedance measurement range 0.01 mΩ - 100 MΩ, basic accuracy 0.05%) at a constant intensity of 100 µA, in the frequency range 0.1-1000 kHz. In this range, 59 measurements equidistant in logarithmic scale were taken.

A conductive measuring cell with two electrodes was used for impedance measurements. Fig. 1 shows the schematic for the measurement method as it was described in a previous paper [42].

Impedance measurements were performed in saturated samples. The prismatic samples were settled vertically, the spaces between electrodes and two opposite faces of mortar were filled with saline solution. The other two faces and the bottom of the sample were sealed with silicone. The solution that was in equilibrium with the mortars was placed as a conductive contact between the sample and the electrodes.

Four impedance measurements were taken at 1.5 cm, 3 cm, 4.5 cm and 6 cm in height. The admittance data (inverse of impedance) were adjusted linearly with the height of measurement to separate the parasitic admittance from the intrinsic admittance of the mortar.

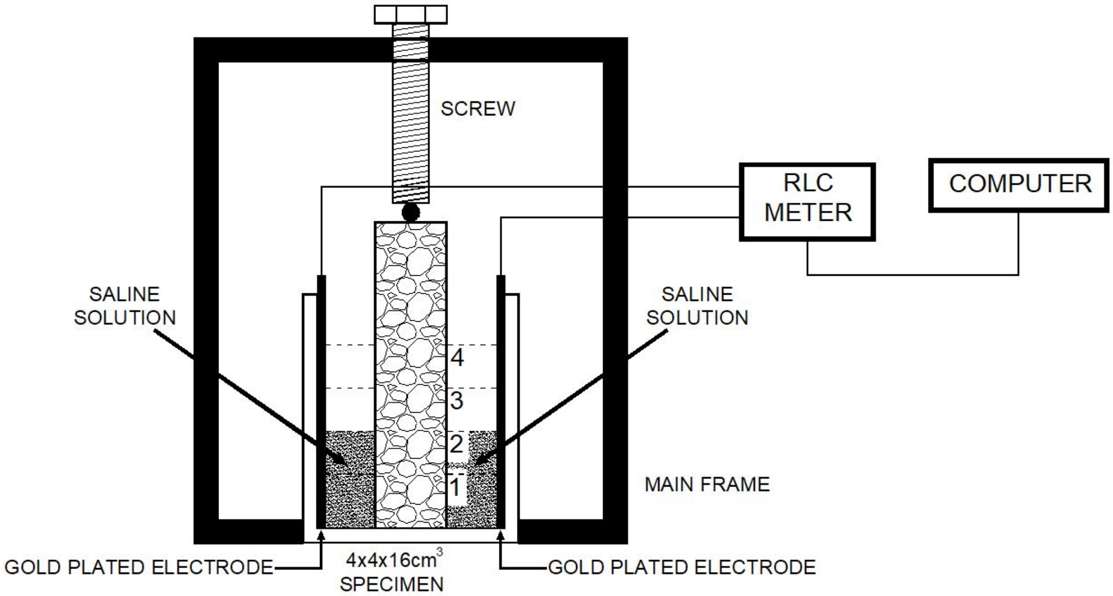

Fig. 1. Schematic view of the two-electrode cell for EIS measurement. Four measuring heights 1.5 cm, 3 cm, 4.5 cm and 6 cm are shown as 1, 2, 3, 4, respectively.

The resulting experimental admittance Y_{ex} was obtained per unit length. The impedance of the mortar Z is in series with the impedance due to the interface electrode-solution-mortar Z_{es} : $Z_{ex} = Z + Z_{es}$. Both impedances were separated by means of an EqC using LEVM software which applies a complex non-linear least squared fitting (CNLS) [60]. The value of the mortar impedance, Z, matches with the electrical resistivity because the geometrical factor resulting for Y_{ex} is the unit (1 m^{-1}).

2.2.2 Drying-rewetting procedure

Two successive processes, at room temperature (20 ºC) and at 50 °C, consisting of six drying-rewetting cycles, were applied to the mortars.

The first and second drying-rewetting cycles, lasting 7 and 14 days, respectively, involved an ambient-drying (AD) process, temperature t = 20 ± 2 ^{o}C and relative humidity RH = (55 ± 3)%, and a subsequent vacuum saturation.

The other four drying-rewetting cycles involved an oven-drying (OD) process at 50 ^{o}C for circa 7 days, until constant weight, and subsequent vacuum saturation.

The vacuum saturation process was performed in two stages: a vacuum extraction during 30 minutes under pressure of 20 mmHg (2.7 kPa) and 1 hour of slow wetting until saturation with distilled water at the same pressure (UNE-EN 1936:2007) [59]. After the saturation process, mortar samples were immersed in distilled water for at least 24 hours before taking the impedance measurements, to ensure the equilibrium between the mortar and saline solution. This solution was used in the impedance measurement.

The nomenclature of the experiment is as follows: Sj, being j=0,1,2,..6 for each of the seven saturated states. The first saturated state, S0, corresponds to the original mature mortar of 270 days, vacuum saturated. The dried states are referenced as: XDj, being j = 1, 2,…6 the number of drying-rewetting cycles, and X = A, O depending on whether they result from drying at AD or OD conditions, respectively. Table 1 shows the nomenclature used during the experiment.

Process State		Ambient Drying (AD)		Oven Drying (OD)			
Dried		AD1	AD2	OD3	OD4	OD5	OD6
Saturated	S0	S1	S2	S3	S4	S5	S6

Table 1 Nomenclature of drying-rewetting states of the mortars and processes.

The water absorbed after saturation in each cycle (XDj-Sj) was measured as a percentage of sample volume W_a. The impedance measurements were taken in every saturated state S0, S1, S2, S3, S4, S5 and S6.

3. RESULTS AND DISCUSSION

3.1 Water removed during the drying-rewetting cycles

Fig. 2 shows the amount of water absorbed W_a at each cycle of the process between the dry state (XDj) and the subsequent saturated state (Sj). In each cycle, XDj-Sj (j=1-6 and X=A,O), the same drying strength for all mortars was applied, and all water inside the pores above a minimum size was removed. The minimum accessible pore size reached at OD conditions was smaller than at AD conditions.

The mass of the samples was approximately the same in all saturated states. In all cycles, the same amount of water that was removed in the drying was recovered in the re-saturating W_a, highlighting the good repeatability of the experiment. The mass in the dry states decreased for successive cycles, and therefore W_a increased from AD1-S1 to OD6-S6 continuously. The continuous increase indicates that in each new cycle water was absorbed into new porosity and that this new accessible porosity appeared after the drying process.

In the two AD cycles, AD1-S1 and AD2-S2, W_a did not exceed 5% in any mortar, although the repetition of the cycle with double time of drying (14 days) caused an increase in W_a from 2.1%, 2.2%, and 3.1% up to 3.3%, 4.0%, and 5.1% for mortars m040, m050, and m060, respectively (Table 2).

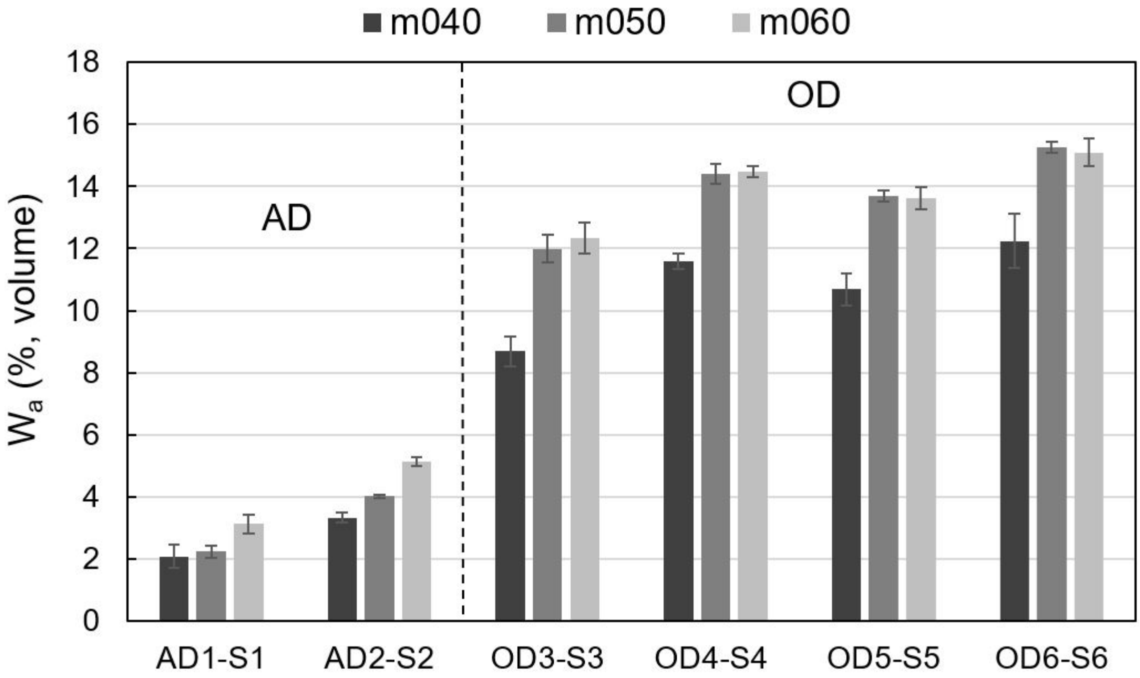

Fig. 2. Water absorbed W_a (percentage in volume) for OPC mortars with w/c = 0.40, 0.50 and 0.60 in ambient drying (AD) cycles (AD1-S1, AD2-S2) and oven drying (OD) cycles (OD3-S3, OD4-S4, OD5-S5, OD6-S6).

By applying the Powers model [10] and assuming that: i) the degree of hydration of cement is 0.85, ii) the intrinsic porosity of the gel C-S-H is 26% and iii) the mortars have 42% of cement paste, the calculated capillary porosity (CaP) is 4%, 7%, and 9% (in volume) for mortars m040, m050, and m060, respectively (Table 2). Therefore, water of CaP was not completely removed during the AD process, only 83%, 57% and 57% of Cap, for m040, m050 and m060, respectively, was involved in AD process. These values show a higher percentage of depercolated CaP in mortars m050 and m060 than in m040, because all water in accessible CaP (>8 nm) is removed at AD conditions [10].

	W_a (%)						CaP	CaP+GeP
Mortars	AD1-S1	AD2-S2	OD3-S3	OD4-S4	OD5-S5	OD6-S6	(%)	(%)
m040	2.1	3.3	8.7	11.6	10.7	12.2	4	13
m050	2.2	4.0	12.0	14.4	13.7	15.2	7	17
m060	3.1	5.1	12.3	14.5	13.6	15.1	9	20

Table 2 Water absorbed W_a (%) shown in Fig. 2, in ambient drying (AD) cycles (AD1-S1, AD2-S2) and oven drying (OD) cycles (OD3-S3, OD4-S4, OD5-S5, OD6-S6). Calculated capillary porosity CaP (%) and total porosity CaP+GeP (%) (Powers model) for the three mortars. Percentages in volume. The uncertainties of W_a are shown in Fig. 2.

According to Jennings et al. [10], by applying the WVSI technique, the large gel pores (4 to 8 nm in diameter) are emptied at RH ≈ 50% and temperature of 24 ºC. Therefore, it is possible that some water of GeP, specifically the water of GeP located on the surface of the sample, might have been removed during the AD cycles.

In the third cycle of the experiment (OD3-S3), which corresponds to the first cycle at 50 °C of OD process, W_a increased more than double, and reached up to 8.7% for m040, 12.0% for m050 and 12.3% for m060.

Returning to the Powers model, the calculated total porosity CaP+GeP was 13%, 17%, and 20% (in volume) for mortars m040, m050, and m060, respectively (Table 2). These values of estimated total porosity agree with data for w/c=0.50 mortars, whose loss of water during OD treatment at 60 ºC was 16% [3]. Therefore, in the first OD cycle the water of GeP was not completely removed. Furthermore, it is possible that the isolated capillary pores pertaining to depercolated CaP remain filled of water.

During the second OD cycle, OD4-S4, W_a increased with respect to the first, OD3-S3, although the same intensity of drying was applied. This result indicates that the repetition of the drying process induced rearrangements in the microstructure that increased the accessible porosity for water [2,4,5,10,17].

A significant decrease in W_a between cycles OD4-S4 and OD5-S5 is observed in all mortars. This result is meaningful because is directly related to a decrease in the electrical conductivity G2, associated to GeP that will be discussed below in the section about electrical properties. This decrease of W_a probably is due to the fact that drying time did not last enough, and only a transient constant weight was reached.

A remarkable feature is that W_a shows the same value for m050 and m060 throughout the OD treatment, in the range 12%-15%, well above the range 9%-12% for m040 (Table 2). Furthermore, at the end of the experiment, W_a reached values of 94%, 89% and 76% of their total porosity, in increasing order of w/c: 0.40, 0.50 and 0.60. These results confirm that mortars with higher w/c ratio have more volume of inaccessible small pores in GeP, and this larger quantity of small pores increases the depercolated CaP; therefore, the OD treatment could not remove the inaccessible water contained in both spaces. Mature m060 has more porosity inaccessible than m050 but the accessible porosity throughout OD process at 50 ºC is the same.

The increase of W_a in the AD process was not due to a change in the microstructure, as will be seen in the section on electrical properties, but to a greater emptying of the CaP due to an increase in drying time.

The increase of W_a from OD2-S2 to OD3-S3 was due to the increase in the intensity of drying from 20 ºC to 50 ºC and the consequent decrease in the minimum size accessible pore.

The successive increase in W_a from the first OD3-S3 to the last OD6-S6, was due to the repetition of the cycle: drying (50 ºC) - rewetting, that caused the successive shrinkage of the solid part of the mortar (small pores of gel C-S-H) and the increasing in size of neighbour pores (largest pores of GeP and smallest pores of CaP). These new pores that exceeded the minimum accessible pore size at 50 ºC, were generated in a drying and were filled in the following rewetting. Therefore, W_a increased with the number of cycles, showing the effect known as pores coarsening [2,4,17]. The successive OD cycles at 50 ^{o}C modified the microstructure of the gel C-S-H as it will be demonstrated by the analysis of electrical properties.

3.2 Impedance data and proposed EqC

Fig. 3(a) shows, as example of data set, the Z-plot (Nyquist plot) of the experimental impedance Z_{ex} for mortar m060 in the seven saturated states (S0-S6) of the experiment.

Every plot shows a small tail on the right, representing the impedance of interface between the electrodes and the sample at low frequencies, in the range 100 Hz - 5 kHz. The rest of the graph, in the range of frequency from 5 kHz to 1 MHz, displays two sub-arcs representing one complete relaxation and the beginning of a second one. An increase in both $Re(Z_{ex})$ and $|Im(Z_{ex})|$ is observed from S0 to S6. Furthermore, the minimum value of $|Im(Z_{ex})|$ increases with the number of cycles. This feature makes essential a fitting to an EqC in order to separate the electrode effects and identify the real part of Z at zero frequency or dc conditions.

Fig. 3(b) shows the series EqC: R_{sol} Q_e (R_1Q_1) (R_2Q_2) for fitting the experimental impedance data. The right part of the circuit R_{sol} Q_e corresponds to the impedance at the electrode-solution interface $Z_{es,}$ simulating the tail at low frequencies (Fig. 3(a)). The left part of EqC represents the impedance of the mortar in the frequency range of the experiment (100 Hz - 1 MHz) with two distributed relaxations of type (RQ) composed by two electrical resistances, R_1 and R_2, and two constant phase elements, Q_1 and Q_2. Each Q is characterized by two electrical parameters: the frequency exponent, n, and the admittance factor, $Y_{0.}$

Kramers-Kronig requirements were tested by fitting impedance data to a Voigt circuit with seven pairs (RC) in series, prior to adjusting the impedance data to EqC. Only those data that exhibited a random scatter of residuals were selected for the analysis.

The calculated statistical parameters of fitting for both, Voigt circuit and two-distributed-relaxations EqC (Fig. 3(b)), for every data set in the experiment were:

1) root mean square values of the estimated relative standard deviation of the fit residuals (PDRMS) that was less than 0.021, 2) residuals with respect to the model (Res/Mod) that were less than 5%, and 3) relative standard deviation of the fit residuals (SF) that was less than 0.016.

These good statistical parameters indicate that the proposed electrical model, with (R_1Q_1) and (R_2Q_2) in series, represents appropriately the electrical impedance of the saturated mortar, both in its original mature state and after the drying-rewetting cycles.

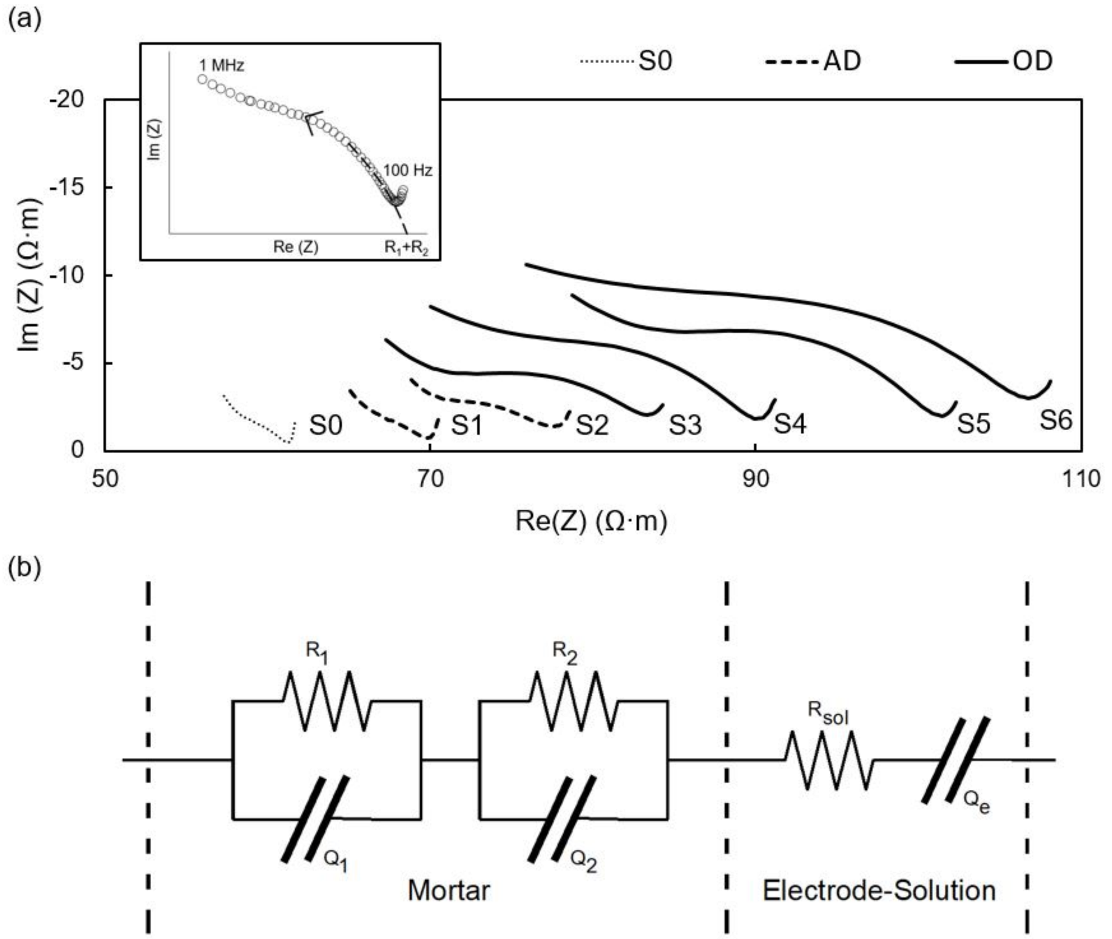

Fig. 3. Impedance data and equivalent circuit (EqC): (a) Nyquist plot of Z_{ex} ($Re(Z_{ex})$ vs $Im(Z_{ex})$) for m060 in their original saturated state S0 and in their saturated states: S1, S2 (ambient drying, AD), and S3, S4, S5, S6 (oven drying, OD), (b) EqC composed of two pairs (R_1Q_1), (R_2Q_2) in series with two elements R_{sol} Q_e. Inset: Any curve of Nyquist plot. Bulk resistance R_1+R_2 is the intersection of the mortar curve at low frequency with the $Re(Z_{ex})$ axis. Arrow points towards increasing frequency.

A key point of IES studies is the microstructural interpretation of the electrical results.

The bulk electrical resistance of the mortar is R_1+R_2 (Inset of Fig. 3(a)). In Nyquist plot $Re(Z_{ex})$ decreases from R_1+R_2 to $Re(Z_{ex}(1\ MHz))$ with frequency. This decrease means an impedance relaxation. $Im(Z_{ex})$ increases and decreases with frequency. The maxima of $\left| Im\ (Z_{ex}) \right|$ show the characteristic frequencies F around which relaxations spread. Only if these characteristic frequencies are significantly different they can be identified by adjusting the EqC.

The impedance and its inverse, the admittance, are complex magnitudes that henceforth are equivalent to resistivity and conductivity, respectively, because the geometric factor of the sample that represents Z_{ex} is the unit.

The two relaxations (R_1Q_1) and (R_2Q_2) have their characteristic frequency F_1 and F_2, respectively, around which different ionic conduction phenomena occur. The frequencies F_1 and F_2 are related to the characteristic time constants T_1 and T_2, defined in Eq (2), with the relationship $2\pi \cdot T_i \cdot F_i = 1$.

Each relaxation is characterized by 3 parameters: R, Y_0 and n. According to the literature on EIS applied to HCB materials, the only electrical parameter that characterizes the impedance relaxation of gel C-S-H is the exponent n with values around 0.80 [26,50,51].

Furthermore, the admittance of each relaxation (RQ) is defined as the sum of two admittances in parallel Y(R) and Y(Q). The admittance Y(Q) in turn is the sum of its real and imaginary parts defined in Eq (1). Therefore, the ionic conductivity associated with each relaxation has three additive components: 1) G (= 1 / R) is in phase with the applied voltage and independent of the frequency of the applied voltage, 2) Re(Y(Q)) of Eq (1a), is in phase with the voltage but dependent on the frequency, and 3) Im(Y(Q)) of Eq (1b), is out of phase π / 2 rad with the voltage and also dependent on the frequency.

These properties of the conductivities allow to associate them to different spaces of the microstructure. Conductivity G is related to the bulk solution of the pore space, and Re(Y(Q)) and Im(Y(Q)) are related to the surface of the pores.

According to the literature, the dispersive elements Q_1 and Q_2 represent the conduction in the surface of the pore, which is due to diffusion and polarization in the electrochemical double layer close to the solid wall of the pores [26,61-63]

Changes in these electrical parameters will allow to relate them to changes in the microstructure.

3.3 Equivalent circuit parameters in the original saturated state S0

Table 3 shows the parameters of EqC (Fig. 3(b)) obtained in the state S0 for the three mortars (mean value of 3 samples). The parameters (R_1, Y_{01}, n_1) and (R_2, Y_{02}, n_2) characterize the two mortar relaxations. Conductivities G_1, G_2 and bulk dc conductivity of the mortar G_{eq} (= $1/(R_1+R_2)$) are also shown in Table 3.

Being n_2 = 0.80-0.83 and $G_2 << G_1$, relaxation (R_2Q_2) can be associated to GeP and therefore (R_1Q_1) to CaP.

Moreover, G_{eq} is in the range of 10-17 mS/m for the three mortars, with their original pore solution. This value is much lower than 150 mS/m, accepted limit value below which the capillary porosity is depercolated [1]; and therefore it can be assumed that the two porosities, CaP and GeP, were arranged in series throughout the path of the ionic species.

		Q_1			Q_2				
S0	R_1 (Ω·m)	Y_{01} ($\Omega^{-1}\cdot s^{n1}$)	n_1 (-)	R_2 (Ω·m)	Y_{02} ($\Omega^{-1}\cdot s^{n2}$)	n_2 (-)	G_1 (mS/m)	G_2 (mS/m)	G_{eq} (mS/m)
m040	0.96	$4.18\cdot10^{-3}$	0.496	93.24	$5.79\cdot10^{-9}$	0.803	1042	10.7	10.6
m050	3.14	$2.63\cdot10^{-3}$	0.463	67.61	$5.23\cdot10^{-9}$	0.825	318	14.8	14.1
m060	4.13	$2.96\cdot10^{-4}$	0.555	57.08	$6.38\cdot10^{-9}$	0.823	242	17.5	16.3

Table 3 Mean values (three samples for each mortar) of the EqC parameters: R_1, Y_{01}, n_1 (of Q_1), R_2, Y_{02}, n_2 (of Q_2) obtained for every mortar at the beginning of the experiment S0 (original saturated 270-day mortar). Calculated dc conductivities: G_1 (=1/R_1), G_2 (=1/R_2) and bulk conductivity $G_{eq} = (R_1+R_2)^{-1}$. The uncertainties of the parameters were about 3% for Y_{02}, 1% for R_1 and Y_{01}, 0.2% for n_1 and n_2, and 0.05% for R_2.

Resistances R_2 and R_1 are associated to GeP and CaP, respectively. The resistance R_2 were 15, 20 and 90 times higher than R_1 for m060, m050, and m040, respectively. These resistances represent the ionic conduction within the volume of the pore and they are related to: 1) the shape and dimensions of the pore, 2) the volume of mortar occupied by the pores and 3) the dc conductivity of the solution that saturates the pores. The relationship between the resistances (R_1, R_2) and the pores size that they represent can not be established only with electrical measurements. It would be necessary to know the dc conductivity of their respective solutions.

The parameter Y_{02} was 5-6 orders of magnitude smaller than Y_{01}. They represent the amplitude of conductivity at the interface for $\omega^n \sim 1$ (about 1 Hz for both, Q_1 and Q_2). Exponent n_2 was about 0.80 and n_1 was about 0.50. With de values obtained for Y_0 and n, in state S0, the conductivity at the pore surface for all mortars ($Y_0 \cdot \omega^n$) was about 10^3 times greater in the pores represented by Q_1 than in those represented by Q_2, in the frequency range from 100 Hz to 1 MHz.

The large difference in conductivity associated with the surface of the pores reaffirms the idea that there are two types of conductive pores with very different surfaces. Element Q_2 corresponds to GeP associated to gel C-S-H and Q_1 is related to CaP.

In HCB materials, an impedance relaxation with an exponent n in the range 0.80-0.82 has been reported [26,50,51]. It has been related to the fractal surface dimension d_f of the C-S-H gel by means of the equation $d_f = 2 \cdot n_2 + 1$ [64]. For the three mortars in the original state S0, with $n_2 = 0.80\text{-}0.83$, the calculated fractal parameters were $d_f = 2.60\text{-}2.66$ that are in agreement with those measured by other techniques for the C-S-H gel [5,18,65].

The characteristic time constant T_i of the (R_iQ_i) relaxation, displayed in Eq (2), indicates the characteristic frequency $F_i = (T_i \cdot 2\pi)^{-1}$ at which the imaginary part of the conductivity reaches approximately the same value as the real part.

Applying Eq (2) for (R_1Q_1) and (R_2Q_2) data, the characteristic time constants were $T_1 \approx 10^{-5}$ s and $T_2 \approx 10^{-8}$ s. The estimated characteristic frequencies were $F_1 \approx 16$ kHz and $F_2 \approx 16$ MHz. The frequency F_2 determined by the parameters of the relaxation (R_2Q_2) although exceeded the highest frequency applied in the experiment and despite representing an incomplete relaxation, agrees with data presented in other articles [54,66].

3.4 Evolution of EqC parameters

In this section, the evolution of the EqC parameters between the saturated states S0 and S6 are analysed for all mortars.

Fig. 4 depicts the values of R_2 and R_1, the resistances associated to GeP and CaP, respectively. The resistance R_2 exhibited significant differences between mortars, in increasing order: m060, m050 and m040. Therefore, R_2 behaves like a parameter that characterizes the w/c ratio. Resistance R_1 had greater uncertainty than R_2 and did not show significant differences between mortars throughout the experiment.

In the AD process, from the original state S0 to S2, both R_1 and R_2 increased. There is a linear relationship between them with determination coefficients higher than 0.85 (graphs not shown), indicating that their increase was due to the same effect.

Both resistances increased in the AD process because the rewetting process was performed with distilled water. The conductivity of the new solution was lower than the original one because some of the precipitated salts did not dissolve. If the saturation had been done with the original saline solution, the resistances would have decreased [20].

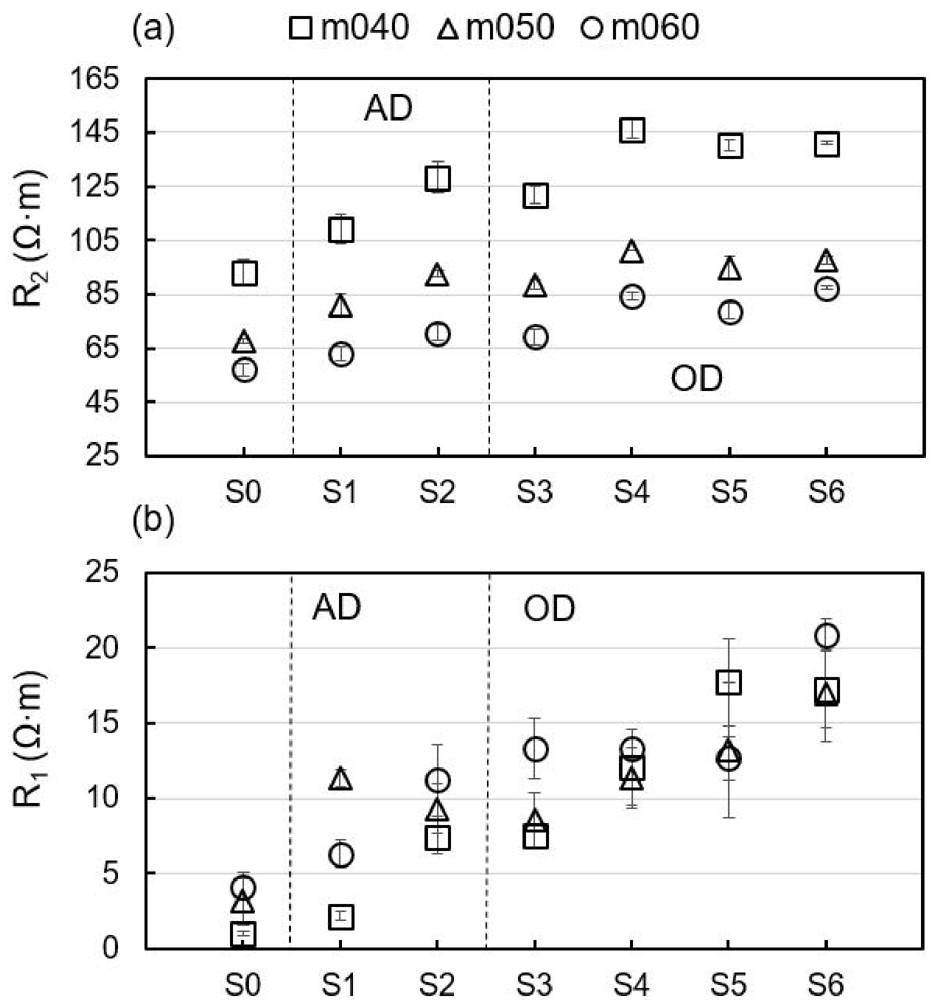

Fig. 4. Resistance R_2 (a) and R_1 (b) for all studied OPC mortars (w/c=0.40-0.50-0.60) at the initial state of saturation, S0, and after successive drying-rewetting cycles. Saturated states S1, S2 (ambient drying, AD) and S3, S4, S5, S6 (oven drying, OD). The units of R_1 and R_2 are Ω·m because the geometrical factor of experimental impedance Z_{ex} is 1 m^{-1})

The resistance R_2, associated to GeP, also increased in the AD process, despite none or very few water of GeP was removed in the AD cycles (W_a% < CaP% in AD process). Nevertheless, this increase of R_2 indicates that the presence of distilled water in CaP affected the solution in pores of GeP after the vacuum-saturation process.

Between the states S2 and S3 there was no significant variation of R_2, although in S3 a considerable increase in W_a was observed (Table 2). Resistance R_2 peaked in S4 for every mortar, and it hardly exhibited any change in the subsequent states, while R_1 increased continuously.

No relationship was observed between R_1 or G_1 and W_a, but it was found between G_2 and W_a. Fig. 5 shows this relationship between the conductivity G_2 associated to GeP and water absorbed W_a.

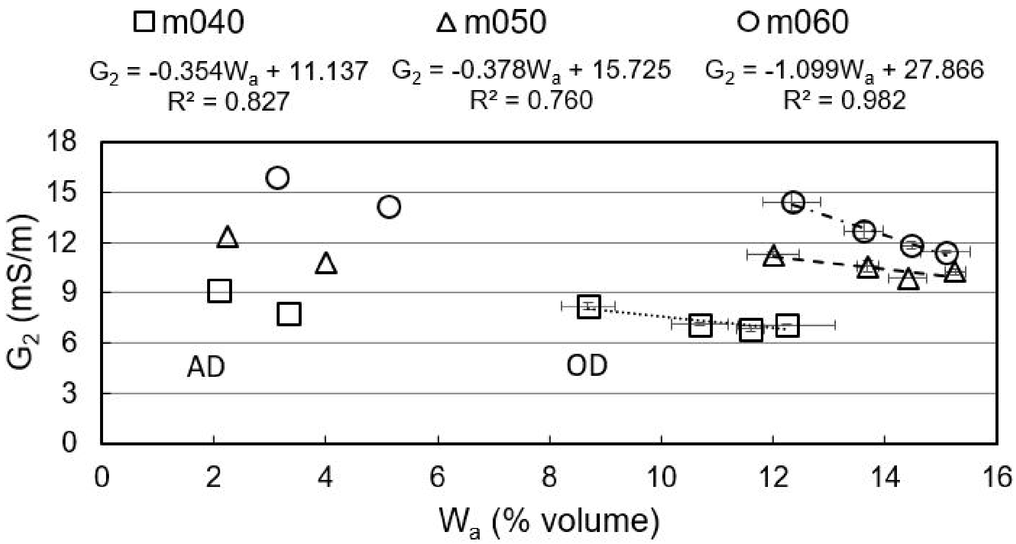

Fig. 5. Relationship between conductivity G_2 and water absorbed W_a for all mortar in saturated states S1, S2 (ambient drying, AD) S3, S4, S5 and S6 (oven drying, OD). Linear equations G_2-W_a and the determination coefficients R^2 for each mortar in the four OD cycles.

In the two processes, AD (W_a < 6%) and OD (W_a > 8%), the conductivity associated to GeP decreased with W_a with a similar behaviour. This suggests that the electrical conductivity of the pore solution decreased in both processes. In the OD cycles, the conductivity of mortar decreased linearly with W_a, as shown in the linear fittings (Fig. 5).

However, between the last AD cycle and the first OD cycle, there was a large increase in W_a, 7% for m060, 8% for m050 and 5% for m040, without a decrease in the conductivity. This confirms the idea that in the first OD cycle at 50 °C, some structural changes were produced in the gel C-S-H, compensating the decrease in the conductivity of the solution.

This behaviour agrees with the coarsening of pores involved in the conductivity [4-6, 17]. The smallest pores got closer due to the shrinkage of the C-S-H gel and neighbour pores became larger, which increased the accessible porosity. These largest pores provided a new path for the ionic current.

From S3 to S6 the coarsening continued but did not compensate the decrease in conductivity of pore solution.

The absence of relationship between R_1 and W_a may be due to the fact that R_1 can be related to different spaces of the mortar matrix, among them the zone that surrounds the aggregates (interfacial transition zone, ITZ), which presents a wide variety in size and shape.

Fig. 6 shows the resistance R of the seven (RC) of the Voigt circuit as a function of the characteristic frequency of each single relaxation (RC). The values correspond to mortar m060 in six saturated states. The circuit was applied to check Kramers-Kronig conditions.

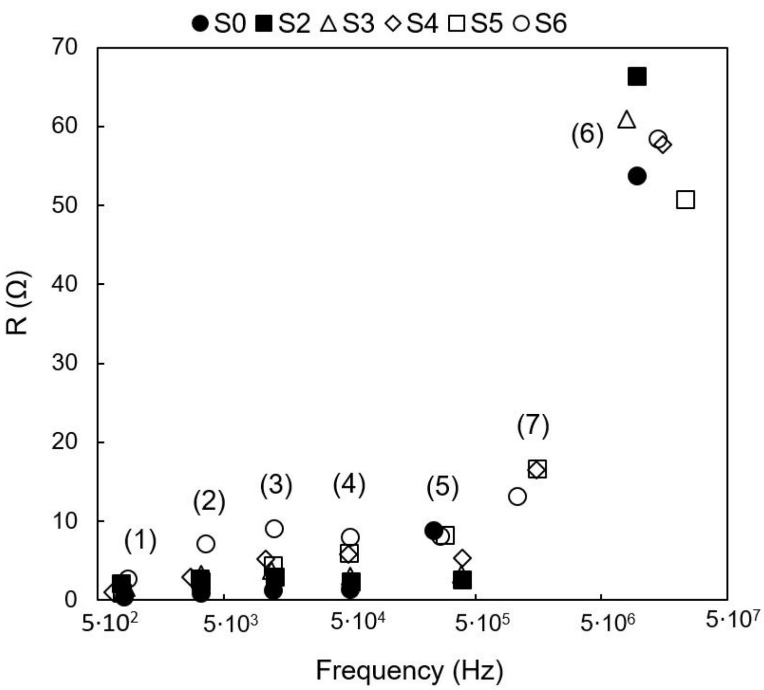

Fig. 6. Resistance R of seven (RC) of Voigt circuit (1) - (7) versus characteristic frequency of each (RC). Values for m060 in six saturated states. Full symbols for S0 and ambient drying (AD) cycle (S2) and open symbols for oven drying (OD) cycles (S3, S4, S5, S6). The (RC) number (7) appears only in the last states S4, S5 and S6.

The largest resistances were obtained for (RC) number (6), with values between 50 Ω and 70 Ω. This range of values is the same as that of the resistance R_2 of (R_2Q_2), which was related to GeP (60-85 Ω in Fig. 4 for m060). These values of R correspond with single relaxations whose characteristic frequency is between 10 MHz and 20 MHz, around $F_2 \approx 16$ MHz which was assigned to the distributed relaxation (R_2Q_2). This result confirms the existence of a frequency of relaxation above the frequency range of measurements that characterizes a homogeneous phase, the gel C-S-H.

Conversely, in the frequency range $5 \cdot 10^2$-$5 \cdot 10^5$ Hz, five Debye relaxations around the characteristic frequency $F_1 \approx 16$ kHz of (R_1Q_1) were found. If their five resistances determine R_1 of distributed relaxation (R_1Q_1), which was associated to CaP, it can be state that this CaP represents a heterogeneous phase. This may be the reason because R_1 is not directly related to the W_a, unlike it is R_2.

In Fig. 7 the exponents n_2 and n_1 of Q_2 and Q_1, associated to GeP and CaP, respectively, are shown.

Exponent n_2 shows a similar value for all mortars throughout the experiment, with a small uncertainty. This exponent changed in the same way for all mortars, indicating that the surface of GeP pores suffered the same change in the OD process, regardless of the w/c ratio.

In the two states of AD process, S1 and S2, the exponent n_2 was around 0.80, the same value as in the original state, S0. This result indicates that the surface of the pores of the C-S-H gel did not change during the AD cycles. This behaviour is in accordance with the fact that the volume of water removed in the AD process (3.3%, 4.0% and 5.1% for m040, m050 and m060, respectively), was smaller than the free water of CaP (4%, 7% and 9%, respectively), and that the AD rewetting process did not affect the surface of the GeP pores.

During the OD process, n_2 decreased monotonously from 0.80 to a value around 0.50. This indicates, from the electrical point of view, that the width of the relaxation (R_2Q_2) increased. From the physical point of view, the conductivity in the ionic layer close to the wall of the pores depends to a lesser extent on the frequency (Eq (1)). The fractal parameter d_f associated to n_2 decreased from 2.60 to 2.00. This decrease is in agreement with the variation of the number of SiO_4 tetrahedral chains linked to the CaO sheets of the C-S-H gel [65] and it is related to the polymerization of the gel that is a consequence of thermal treatments [67]. In other studies where a decrease of n_2 from 0.80 to 0.60 was observed, the pore solution was replaced by NaCl solutions, and likely the effect of Na+ on Ca-sheets of gel C-S-H was similar to the one observed in the OD process [41].

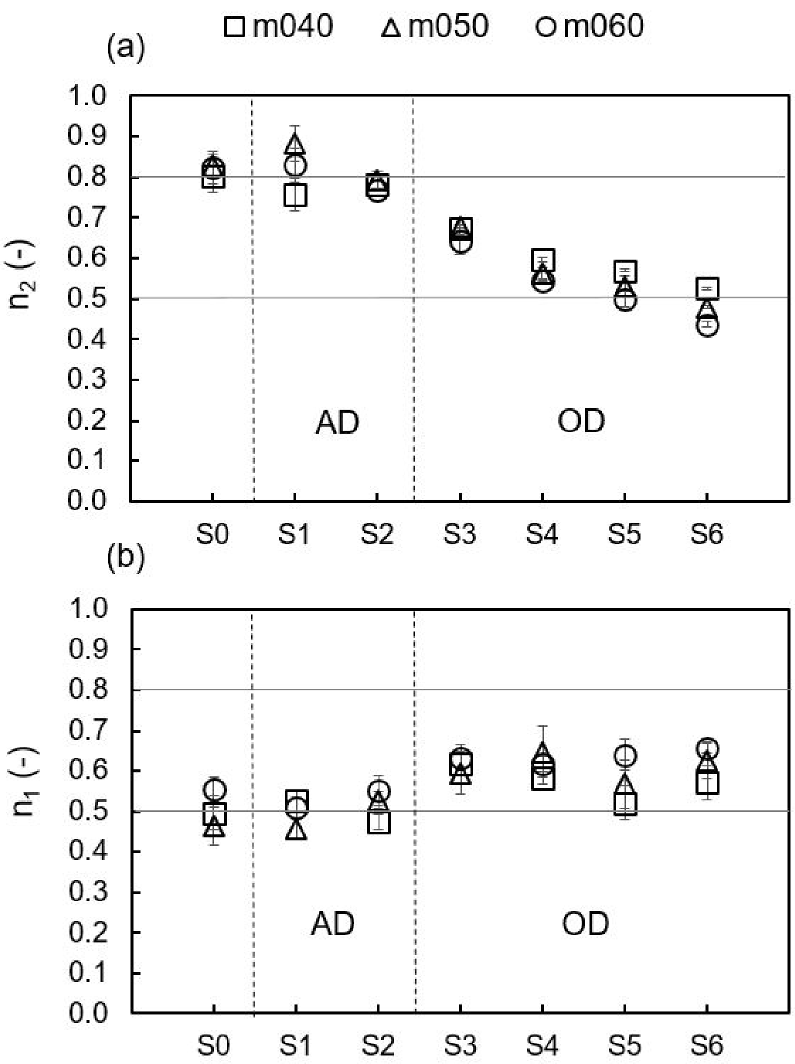

Fig. 7. Evolution of Q_1 and Q_2 exponents (a) n_2, (b) n_1 during the successive drying-rewetting cycles for every type of studied OPC mortar (w/c = 0.40-0.50-0.60). Initial state S0 and successive states S1, S2 (ambient drying, AD) and S3, S4, S5, S6 (oven drying, OD).

Exponent n_1 also shows a value similar to all mortars throughout the experiment. However, this behaviour is very different from n_2. In the first states S0, S1 and S2 (AD), n_1 showed a value around 0.50. The constant value of n_1 in AD process indicates no effects or reversible effects on the surface of the CaP. In the first cycle of the OD process, n_1 increased to values around 0.60 and remained constant until the end.

The effect of the drying-rewetting process was different for the two relaxations. The repetition of the OD cycles did not affect significantly the n_1 exponent associated to CaP, unlike the n_2 exponent associated to GeP, which decreased continuously.

The values of Y_{02} and Y_{01}, corresponding to Q_2 and Q_1, associated to GeP and CaP, respectively, are depicted in Fig. 8.

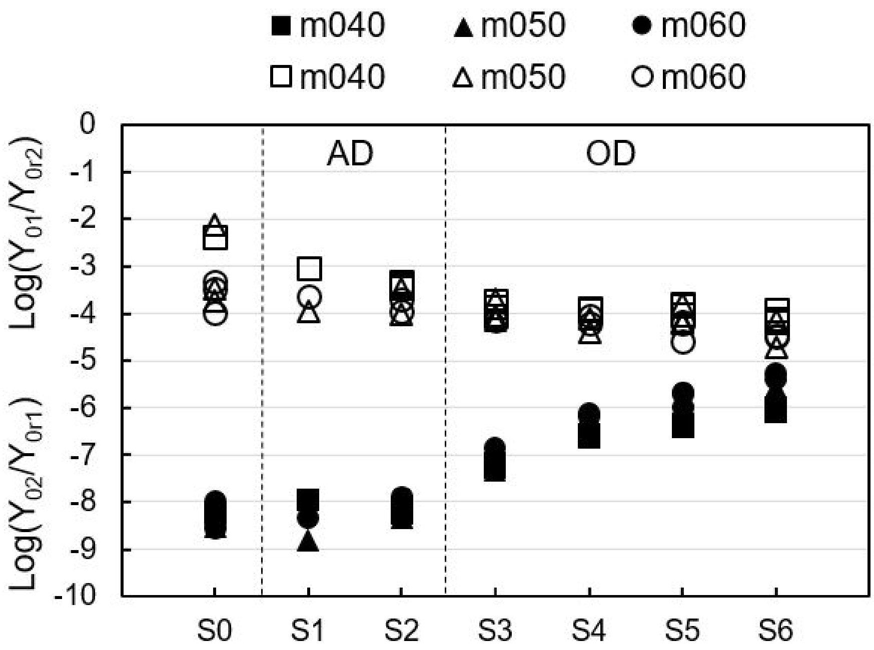

Fig. 8. Evolution of $\log(Y_{01}/Y_{0r})$ and $\log(Y_{02}/Y_{0r})$ during successive drying-rewetting cycles for every studied OPC mortar (w/c = 0.40-0.50-0.60). $Y_{0r1} = Y_{0r2} = 1$ ($\Omega^{-1}\cdot s^n$) is a reference value (for units n = n_1, n_2, respectively). Original saturated state S0, S1 S2 (ambient drying, AD), and S3, S4, S5, S6 (oven drying, OD). Full symbols for Y_{02} and open symbols for Y_{01}.

In the AD process (states S1, S2), the values of Y_{02} and Y_{01} hardly changed, having a difference about 4-5 orders of magnitude between them. In the OD process, Y_{01} decreased slightly, around one order of magnitude, whereas Y_{02} increased 2-3 orders of magnitude.

The evolution of surface conductivities, between the original state S0 and the last state of the experiment S6, is summarized in Fig. 9. Calculated values for m050 are shown as an example.

Both, real and imaginary part of admittance (conductivity) are shown, between 100 Hz and 1 MHz. The conductivity represented by Q_1 is 1000 times greater than Q_2 (units in S and mS, respectively).

The decrease in Y_{01} and increase in n_1 result in a decrease of the surface conductivity associated to CaP by approximately 50% (Fig. 9 (a)). The increase in Y_{02} and the decrease in n_2 result in a rise of the surface conductivity associated to GeP approximately 10 times from the initial S0 to last state S6 (Fig. 9 (b)). This increase in surface conductivity is the consequence of a smoothing of the pores surface in GeP. These pores are the result of the coarsening effect.

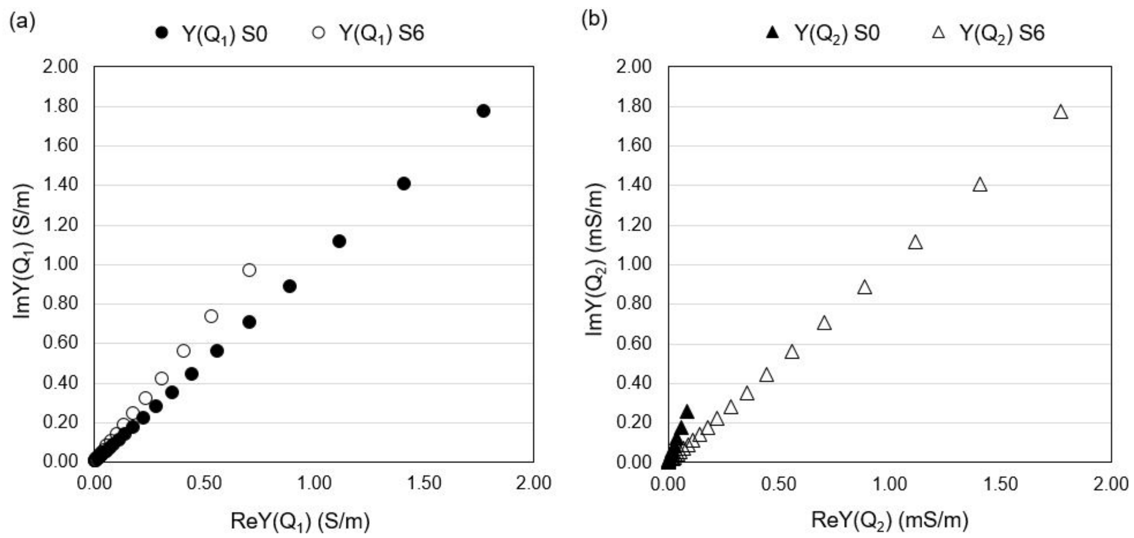

Fig. 9. Imaginary part of admittance Im(Y(Q)) versus real part Re(Y(Q) (or conductivity) for Q_1 (a) and Q_2 (b), in the range from 100 Hz (lower values) to 1 MHz (higher values), in the first saturated state S0 (full symbols) and the last saturated state S6 (open symbols). Calculated values with m050 data.

The continuous evolution of the electrical parameters R_1, R_2, n_1, n_2, Y_{01} and Y_{02} demonstrates the suitability of the electrical model used to explain the electrical conductivity of OPC mortars. In addition, the physical meaning of the parameters that define the two relaxations is conserved, and the changes that occurred during the drying-rewetting processes detected by EIS-EqC methodology agree with the changes of the microstructure deduced from W_a measurements.

4. CONCLUSIONS

The main conclusions obtained from the results previously discussed in this work are:

1) The electrical impedance spectroscopy (EIS), in the range from 100 Hz to 1 MHz, enabled detection of changes in the porosity of the mortars subjected to drying-rewetting cycles and distinguished between mortars with different w/c ratios.

2) The physical model that explains the electrical conductivity of saturated mortars with two distributed relaxations of type (RQ) is consistent because it explains the conductivity of mortars in the original state, and after they were subjected to successive drying-rewetting cycles, at two drying levels: 20 ºC (room temperature) and 50 ºC.

3) Although the two relaxations can not be directly related to pores size, because the conductivities of the respective solutions are unknown, electrical parameters of the proposed equivalent circuit allowed to identify two different conductivities associated to gel and capillary porosities.

4) The drying at ambient temperature produced reversible changes in the mortars, while the drying effects at 50 ºC were irreversible. The changes in electrical parameters measured with EIS-EqC methodology agree with the amount of water absorbed and with the microstructural changes reported by other methods.

5) In the drying-rewetting process at room temperature, only the conductivity of the pores solution changed. In the drying-rewetting cycles at 50 °C, the volume of pores detected at 50 ºC increased monotonously (pore coarsening) and the surface of C-S-H gel became continuously more conductive (surface smoothing).

ACKNOWLEDGMENTS

The authors would like to thank the Spanish Ministry of Science and Innovation for supporting this research through the project BIA 2011-26947

REFERENCES

[1] G. Sant, D. Bentz, J. Weiss, Capillary porosity depercolation in cement-based materials: Measurement techniques and factors which influence their interpretation, Cem. Concr. Res. 41 (2011) 854–864. doi:10.1016/j.cemconres.2011.04.006.

[2] H.M. Jennings, J.W. Bullard, J.J. Thomas, J.E. Andrade, J.J. Chen, G.W. Scherer, Characterization and modeling of pores and surfaces in cement paste: correlations to processing and properties, J. Adv. Concr. Technol. 6 (2008) 5–29. doi:10.3151/jact.6.5.

[3] N. Fischer, R. Haerdtl, P.J. McDonald, Observation of the redistribution of nanoscale water filled porosity in cement based materials during wetting, Cem. Concr. Res. 68 (2015) 148–155. doi:10.1016/j.cemconres.2014.10.013.

[4] J.J. Thomas, H.M. Jennings, Effect of Heat Treatment on the Pore Structure and Drying Shrinkage Behavior of Hydrated Cement Paste, J. Am. Ceram. Soc. 85 (2002) 2293–2298. doi:10.1111/j.1151-2916.2002.tb00450.x.

[5] H.M. Jennings, J.J. Thomas, J.S. Gevrenov, G. Constantinides, F.-J. Ulm, A multi-technique investigation of the nanoporosity of cement paste, Cem. Concr. Res. 37 (2007) 329–336. doi:10.1016/j.cemconres.2006.03.021.

[6] I. Maruyama, Y. Nishioka, G. Igarashi, K. Matsui, Microstructural and bulk property changes in hardened cement paste during the first drying process, Cem. Concr. Res. 58 (2014) 20-34. doi:10.1016/j.cemconres.2014.01.007.

[7] A. Gajewicz, E. Gartner, K. Kang, P. McDonald, A 1 H NMR relaxometry investigation of gel-pore drying shrinkage in cement pastes, Cem. Concr. Res. 86 (2016) 12-19. doi: 10.1016/j.cemconres.2016.04.013.

[8] A. Korpa, R. Trettin, The influence of different drying methods on cement paste microstructures as reflected by gas adsorption: Comparison between freeze-drying (F-drying), D-drying, P-drying and oven-drying methods, Cem. Concr. Res. 36 (2006) 634–649. doi:10.1016/j.cemconres.2005.11.021.

[9] D. Snoeck, L. Velasco, A. Mignon, The influence of different drying techniques on the water sorption properties of cement-based materials, Cem. Concr. Res. 64 (2014) 54-62. doi:10.1016/j.cemconres.2014.06.009.

[10] H. Jennings, A. Kumar, G. Sant, Quantitative discrimination of the nano-pore-structure of cement paste during drying: New insights from water sorption isotherms, Cem. Concr. Res. 76 (2015) 27-36. doi:10.1016/j.cemconres.2015.05.006.

[11] J.J. Thomas, A.J. Allen, H.M. Jennings, Structural changes to the calcium–silicate–hydrate gel phase of hydrated cement with age, drying, and resaturation, J. Am. Ceram. Soc. 91 (2008) 3362–3369. doi: 10.1111/j.1551-2916.2008.02636.x.

[12] J.R. Macdonald, Utility of continuum diffusion models for analyzing mobile-ion immittance data: electrode polarization, bulk, and generation–recombination effects, J. Phys. Condens. Matter. 22 (2010) 495101. doi:10.1088/0953-8984/22/49/495101.

[13] A.C.A. Muller, K.L. Scrivener, A.M. Gajewicz, P.J. McDonald, Densification of C–S–H Measured by 1 H NMR Relaxometry, J. Phys. Chem. C. 117 (2013) 403–412. doi:10.1021/jp3102964.

[14] H.M. Jennings, J.J. Thomas, J.S. Gevrenov, G. Constantinides, F.J. Ulm, A multi-technique investigation of the nanoporosity of cement paste, Cem. Concr. Res. 37 (2007) 329–336. doi:10.1016/j.cemconres.2006.03.021.

[15] T. Rougelot, F. Skoczylas, N. Burlion, Water desorption and shrinkage in mortars and cement pastes: experimental study and poromechanical model, Cem. Concr. Res. 39 (2009) 36-44. doi:10.1016/j.cemconres.2008.10.005

[16] R. Vočka, C. Gallé, M. Dubois, P. Lovera, Mercury intrusion porosimetry and hierarchical structure of cement pastes - theory and experiment, Cem. Concr. Res. 30 (2000) 521–527. doi:10.1016/S0008-8846(99)00252-5.

[17] Y. Aono, F. Matsushita, S. Shibata, Nano-structural changes of CSH in hardened cement paste during drying at 50° C, J. Adv. Concr. Tech. 5 (2007) 313-323. doi:10.3151/jact.5.313

[18] Q. Zeng, M. Luo, X. Pang, L. Li, K. Li, Surface fractal dimension: An indicator to characterize the microstructure of cement-based porous materials, Appl. Surf. Sci. 282 (2013) 302–307. doi:10.1016/j.apsusc.2013.05.123.

[19] B.T. Tamtsia, J.J. Beaudoin, J. Marchand, A coupled AC impedance—creep and shrinkage investigation of hardened cement paste, Mater. Struct. 36 (2003) 147–155. doi:10.1007/BF02479553.

[20] J.J. Beaudoin, B. Tamtsia, Effect of drying methods on microstructural changes in hardened cement paste: an AC impedance spectroscopy evaluation, J. Adv. Concr. Tech. 2 (2004) 113-120. doi:10.3151/jact.2.113

[21] B. Dong, J. Zhang, Y. Liu, G. Fang, Z. Ding, F. Xing, Tracing hydration feature of aluminophospahte cementitious materials by means of electrochemical impedance method, Constr. Build. Mater. 113 (2016) 997-1006. doi: 10.1016/j.conbuildmat.2016.03.072

[22] J.R. Macdonald, Impedance spectroscopy: emphasizing solid materials and systems, A Wiley-Interscience Publ. John Wiley Sons, New York. (1987).

[23] W.J. McCarter, A.B. Afshar, Monitoring the early hydration mechanisms of hydraulic cement, J. Mater. Sci. 23 (1988) 488–496. doi:10.1007/BF01174674.

[24] W.J. McCarter, S. Garvin, Dependence of electrical impedance of cement-based materials on their moisture condition, J. Phys. D. Appl. Phys. 22 (1989) 1773–1776. doi:10.1088/0022-3727/22/11/033.

[25] W.J. McCarter, S. Garvin, N. Bouzid, Impedance measurements on cement paste, J. Mater. Sci. Lett. 7 (1988) 1056–1057. doi:10.1007/BF00720825.

[26] A. Berg, G.A. Niklasson, K. Brantervik, B. Hedberg, L.-O. Nilsson, Dielectric properties of cement mortar as a function of water content, J. Appl. Phys. 71 (1992) 5897–5903. doi:10.1063/1.350488

[27] B.J. Christensen, T.O. Mason, H.M. Jennings, D.P. Bentz, E.J. Garboczi, Experimental and Computer Simulation Results for the Electrical Conductivity of Portland Cement Paste, MRS Proc. 245 (1991) 259. doi:10.1557/PROC-245-259.

[28] P. Gu, Z. Xu, P. Xie, J.J. Beaudoin, Application of A.C. impedance techniques in studies of porous cementitious materials: (I): Influence of solid phase and pore solution on high frequency resistance, Cem. Concr. Res. 23 (1993) 531–540. doi:10.1016/0008-8846(93)90003-R.

[29] P. Gu, P. Xie, J.J. Beaudoin, R. Brousseau, AC impedance spectroscopy (II): Microstructural characterization of hydrating cement-silica fume systems, Cem. Concr. Res. 23 (1993) 157–168. doi:10.1016/0008-8846(93)90147-2.

[30] J. Lizarazo-Marriaga, C. Higuera, P. Claisse, Measuring the effect of the ITZ on the transport related properties of mortar using electrochemical impedance,

Constr. Build. Mater. 52 (2014) 9-16. doi: 10.1016/j.conbuildmat.2013.10.077.

[31] V.M. Sanchez-Fajardo, M.E. Torres, A.J. Moreno, Study of the pore structure of the lightweight concrete block with lapilli as an aggregate to predict the liquid permeability by dielectric spectroscopy, Constr. Build. Mater. 53 (2014) 225-234. doi:10.1016/j.conbuildmat.2013.11.093.

[32] B.J. Christensen, T. Coverdale, R.A. Olson, S.J. Ford, E.J. Garboczi, H.M. Jennings, T.O. Mason, Impedance Spectroscopy of Hydrating Cement-Based Materials: Measurement, Interpretation, and Application, J. Am. Ceram. Soc. 77 (1994) 2789–2804. doi:10.1111/j.1151-2916.1994.tb04507.x.

[33] G.A. Brantervik, K. Niklasson, Circuit models for cement based materials obtained from impedance spectroscopy, Cem. Concr. Res. 21 (1991) 496–508. doi:10.1016/0008-8846(91)90099-4.

[34] C. Andrade, V.M. Blanco, A. Collazo, M. Keddam, X.R. Nóvoa, H. Takenouti, Cement paste hardening process studied by impedance spectroscopy, Electrochim. Acta. 44 (1999) 4313–4318. doi:10.1016/S0013-4686(99)00147-4.

[35] B. Dong, Q. Qiu, J. Xiang, C. Huang, H. Sun, F. Xing, W. Liu, Electrochemical impedance interpretation of the carbonation behavior for fly ash-slag-cement materials, Constr. Build. Mater. 93 (2015) 933-942. doi:10.1016/j.conbuildmat.2015.05.066

[36] C.A. Scuderi, T.O. Mason, H.M. Jennings, Impedance spectra of hydrating cement pastes, J. Mater. Sci. 26 (1991) 349–353. doi:10.1007/BF00576526.

[37] B. Dong, Z. Gu, Q. Qiu, Y. Liu, W. Ding, F. Xing, S. Hong, Electrochemical feature for chloride ion transportation in fly ash blended cementitious materials, Constr. Build. Mater. 161 (2018) 557-586. doi:10.1016/j.conbuildmat.2017.11.123

[38] H. Sun, Z. Ren, S. Ali Memon, D. Zhao, X. Zhang, D. Li, F. Xing, Investigation drying behavior of cement mortar through electrochemical impedance spectroscopy analysis, Constr. Build. Mater. 135 (2017) 361-368. doi:10.1016/j.conbuildmat.2016.12.196

[39] M. Cabeza, P. Merino, A. Miranda, X.R. Novoa, I. Sanchez, Impedance spectroscopy study of hardened Portland cement paste, Cem. Concr. Res. 32 (2002) 881–891. doi:10.1016/S0008-8846(02)00720-2

[40] I. Sánchez, X.R. Nóvoa, G. de Vera, M.A. Climent, Microstructural modifications in Portland cement concrete due to forced ionic migration tests. Study by impedance spectroscopy, Cem. Concr. Res. 38 (2008) 1015–1025. doi:10.1016/j.cemconres.2008.03.012.

[41] B. Diaz, L. Freire, P. Merino, X.R. Novoa, M.C. Pérez, Impedance spectroscopy study of saturated mortar samples, Electrochim. Acta. 53 (2008) 7549–7555. doi:10.1016/j.electacta.2007.10.042

[42] J.M. Cruz, I.C. Fita, L. Soriano, J. Payá, M. V Borrachero, The use of electrical impedance spectroscopy for monitoring the hydration products of Portland cement mortars with high percentage of pozzolans, Cem. Concr. Res. 50 (2013) 51–61. doi:10.1016/j.cemconres.2013.03.019.

[43] B. Boukamp, D. Blank, High-precision impedance spectroscopy: a strategy demonstrated on PZT, IEEE Trans. Ultrason. Ferroelectr. Freq. Control. 58 (2011) 2521–2530. doi:10.1109/TUFFC.2011.2115.

[44] Q. Qiu, Z. Gu, J. Xiang, C. Huang, S. Hong, F. Xing, B. Dong, Influence of slag incorporation on electrochemical behavior of carbonated cement, Constr. Build. Mater. 147 (2017) 661-668. doi:10.1016/j.conbuildmat.2017.05.008.

[45] A. Husain, K. Kupwade-Patil, A. F. Al-Aibani, M.F. Abdulsalam, In situ

electrochemical impedance characterization of cement paste with volcanic ash to examine early stage of hydration, Constr. Build. Mater. 133 (2017) 107-117. doi:10.1016/j.conbuildmat.2016.12.054

[46] B.A. Boukamp, J.R. Macdonald, Alternatives to Kronig-Kramers transformation and testing, and estimation of distributions, Solid State Ionics. 74 (1994) 85–101. doi:10.1016/0167-2738(94)90440-5.

[47] B.A. Boukamp, A Linear Kronig-Kramers Transform Test for Immittance Data Validation, J. Electrochem. Soc., 142 (1995) 1885-1894. doi:10.1149/1.2044210

[48] M. Orazem, M.E. Pavan, S. Membrino, Extension of the measurement model approach for deconvolution of underlying distributions for impedance measurements, Electrochim. Acta. 47 (2002) 2027–2034. doi:10.1016/S0013-4686(02)00065-8.

[49] J.R. Macdonald, E. Tuncer, Deconvolution of immittance data: Some old and new methods, J. Electroanal. Chem. 602 (2007) 255–262. doi:10.1016/j.jelechem.2007.01.006

[50] F. Leroux, J. Russias, C. Cau-dit-Coumes, F. Frizon, G. Renaudin, Low-to-Medium-Frequency AC Impedance Spectroscopy Investigations of Nanocrystalline Calcium Silicate Hydrate Dried Powders, J. Am. Ceram. Soc. 94 (2011) 2680–2687. doi:10.1111/j.1551-2916.2011.04429.x

[51] S.S. Yoon, H.C. Kim, R.M. Hill, The dielectric response of hydrating porous cement paste, J. Phys. D. Appl. Phys. 29 (1996) 869.

[52] M. Keddam, H. Takenouti, X.R. Nóvoa, C. Andrade, C. Alonso, Impedance measurements on cement paste, Cem. Concr. Res. 27 (1997) 1191–1201. doi:10.1016/S0008-8846(97)00117-8.

[53] C. Tsonos, I. Stavrakas, C. Anastasiadis, A. Kyriazopoulos, A. Kanapitsas, D.

Triantis, Probing the microstructure of cement mortars through dielectric parameters' variation, J. Phys. Chem. Solids. 70 (2009) 576–583. doi:10.1016/j.jpcs.2008.12.015

[54] W.J. McCarter, H.M. Taha, B. Suryanto, G. Starrs, Two-point concrete resistivity measurements: interfacial phenomena at the electrode–concrete contact zone, Meas. Sci. Technol. 26 (2015) 85007. doi:10.1088/0957-0233/26/8/085007.

[55] D.P. Almond, B. Vainas, The dielectric properties of random R - C networks as an explanation of the `universal' power law dielectric response of solids, J. Phys. Condens. Matter. 11 (1999) 9081–9093. doi:10.1088/0953-8984/11/46/310.

[56] M. Kinka, J. Banys, J. Macutkevic, A. Pöppl, W. Böhlmann, V. Umamaheswari, M. Hartmann, G. Völkel, Dielectric response of water confined in MCM-41 molecular sieve material, Phys. Status Solidi. B-Basic 242 (2005). doi:10.1002/pssb.200541038.

[57] Norma UNE-EN 197-1:2011 http://www.aenor.es/aenor/normas/normas/fichanorma.asp?tipo=N&codigo=N0048623#.WyJiG6czaUk (accessed June 14, 2018).

[58] Norma UNE-EN 196-1:2005 http://www.aenor.es/aenor/normas/normas/fichanorma.asp?tipo=N&codigo=N0034791#.WyJjVaczaUk (accessed June 14, 2018).

[59] Norma UNE-EN 1936:2007 http://www.aenor.es/aenor/normas/normas/fichanorma.asp?tipo=N&codigo=N0038621#.WyJkc6czaUk (accessed June 14, 2018).

[60] J.R. Macdonald, Comparison of Parametric and Nonparametric Methods for the Analysis and Inversion of Immittance Data: Critique of Earlier Work, J. Comput. Phys. 157 (2000) 280–301. doi:10.1006/jcph.1999.6378.

[61] M.-C. Chien, G.-J. Wang, M.-C. Yu, Nanopore Size Estimation by Electrochemical Impedance Spectroscopy Analysis, Jpn. J. Appl. Phys. 47 (2008) 7459–7463. doi:10.1143/JJAP.47.7459.

[62] M.J. Vitarelli, S. Prakash, D.S. Talaga, Determining Nanocapillary Geometry from Electrochemical Impedance Spectroscopy Using a Variable Topology Network Circuit Model, Anal. Chem. 83 (2011) 533–541. doi:10.1021/ac102236k.

[63] W.J. McCarter, S. Garvin, Dependence of electrical impedance of cement-based materials on their moisture condition, J. Phys. D. Appl. Phys. 22 (1989) 1773–1776. doi:10.1088/0022-3727/22/11/033.

[64] G.A. Niklasson, A fractal description of the dielectric response of disordered materials, J. Phys. Condens. Matter. 5 (1993) 4233–4242. doi:10.1088/0953-8984/5/25/013.

[65] J.A. Janik, W. Kurdowski, R. Podsiadły, J. Samseth, Studies of Fractal Aspects of Cement, Acta Phys. Pol. A. 90 (1996) 1179–1184. doi:10.12693/APhysPolA.90.1179.

[66] B. Díaz, L. Freire, P. Merino, X.R. Nóvoa, M.C. Pérez, Impedance spectroscopy study of saturated mortar samples, Electrochim. Acta. 53 (2008) 7549–7555. doi:10.1016/j.electacta.2007.10.042.

[67] J. Thomas, H.M. Jennings, A colloidal interpretation of chemical aging of the C-S-H gel and its effects on the properties of cement paste, Cem.Concr.Res. 36 (2006) 30–38. doi:10.1016/j.cemconres.2004.10.022